ACS APPLIED MATERIALS & INTERFACES

Research Article

www.acsami.org

Alternating Current Dielectrophoresis Optimization of Pt-Decorated Graphene Oxide Nanostructures for Proficient Hydrogen Gas Sensor

Jianwei Wang,[†,#,⊥] Servin Rathi,[†,⊥] Budhi Singh,[†] Inyeal Lee,[†] Han-Ik Joh,[§] and Gil-Ho Kim*[,†]

[†]Samsung-SKKU Graphene Center, Sungkyunkwan Advanced Institute of Nanotechnology (SAINT) and School of Electronic and Electrical Engineering, Sungkyunkwan University, Suwon, Gyeonggi-do 440-746, Republic of Korea

[#]School of Mechanical and Electrical Engineering, Guizhou Normal University, Guiyang 550002, China

[§]Institute of Advanced Composite Materials, Korea Institute of Science and Technology 864-9, Dunsan-ri, Bongdong-eup, Wanju-gun, Jeollabukdo 565-902, Republic of Korea

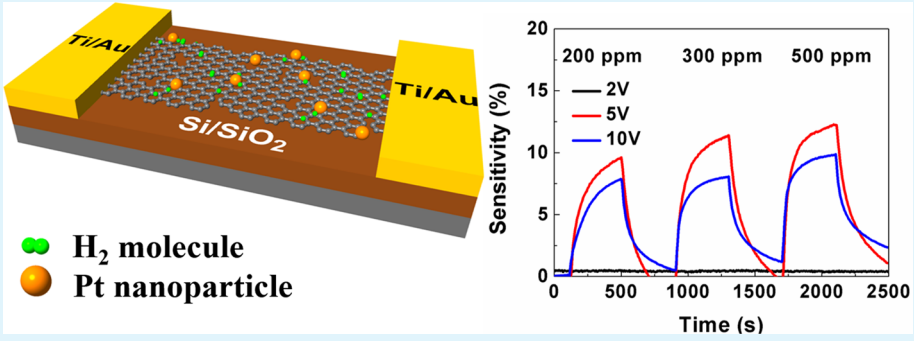

ABSTRACT: Alternating current dielectrophoresis (DEP) is an excellent technique to assemble nanoscale materials. For efficient DEP, the optimization of the key parameters like peak-to-peak voltage, applied frequency, and processing time is required for good device. In this work, we have assembled graphene oxide (GO) nanostructures mixed with platinum (Pt) nanoparticles between the micro gap electrodes for a proficient hydrogen gas sensors. The Pt-decorated GO nanostructures were well located between a pair of prepatterned Ti/Au electrodes by controlling the DEP technique with the optimized parameters and subsequently thermally reduced before sensing. The device fabricated using the DEP technique with the optimized parameters showed relatively high sensitivity (~10%) to 200 ppm hydrogen gas at room temperature. The results indicates that the device could be used in several industry applications, such as gas storage and leak detection.

KEYWORDS: *reduced graphene oxide, Pt nanoparticles, hydrogen gas sensing, dielectrophoresis, nano device*

INTRODUCTION

Hydrogen gas exhibits excellent properties, which have the potential to solve the problems of global pollution and the growing shortage of resources, since it is clean, renewable, and has a wide range of industry applications. Hydrogen gas has been used as an excellent energy carrier in fuel cells, methanol industries, and in power generation. However, hydrogen gas is flammable and can easily explode in air at a concentration of only 4%.[1] Moreover, hydrogen is a colorless and flavorless gas. Therefore, gas sensing techniques for hydrogen gas has become pertinent in the area of sensing research. To fabricate a highly sensitive and stable hydrogen gas sensor, many metal oxide materials, such as ZnO and SnO_2, have been evaluated.[2−4] Recently, carbon-based nanomaterials such as carbon nanotubes have also been evaluated as base materials for hydrogen gas sensors.[5−9] In particular, graphene oxide (GO) exhibits excellent sensing properties for the detection of hydrogen gas. However, the sensing behavior of simple GO-based hydrogen gas sensors can be improved further using hybrid material like nanoparticles or chemical functionalization.[10,11]

To enhance the sensitivity of GO-based hydrogen gas sensors, several methods have been evaluated. Metal decoration with platinum has proved to be an effective method and the hydrogen-gas-sensing properties of graphene or GO materials are significantly improved following Pt decoration. Dielectrophoresis (DEP) is another method for improving the sensing behavior. The DEP technique has gained popularity, since it can precisely locate the nanostructures on the substrate.[12−15] Our previous work and other research reported that the hydrogen gas sensing behavior of GO nanostructures assembled via the DEP technique demonstrate significant improvement in comparison to simple GO-based hydrogen gas sensors.[16−19] However, DEP assembled GO nanostructures with metal decoration have not yet been reported. In this report, we fabricated a hydrogen gas sensor device based on GO nanostructures with Pt nanoparticles, which were assembled using the DEP technique. The Pt-decorated GO

Received: February 10, 2015
Accepted: June 4, 2015
Published: June 4, 2015

DOI: 10.1021/acsami.5b01329
ACS Appl. Mater. Interfaces 2015, 7, 13768−13775

nanostructures were assembled into microgap electrodes by controlling the DEP parameters, such as the applied voltage, applied frequency, and processing time.

EXPERIMENTAL SECTION

The GO nanostructures were synthesized using a modified Hummer's method.[20] First, 4 g of graphite flakes were added to a 250 mL round-bottom flask containing 120 mL of H_2SO_4 that was stirred for 1 h. During stirring, $KMnO_4$ aqueous solution was subsequently added to the mixture every 20 min. The mixture was slowly heated to 40 °C, and the temperature was maintained for 5 h to oxidize the graphite. Subsequently, 150 mL of deionized (DI) water was added to the mixture. The mixture was stirred for 30 min while 17 mL of H_2O_2 solution was added. The mixture was subsequently maintained at 40 °C for 24 h, followed by centrifuging. The resultant mixture was enclosed in a dialysis tube and washed with ultrapure DI water several times to obtain a pH level of 5. The concentration of the GO nanostructures solution was ~1 mg/mL. Figure 1a shows the atomic force microscopy (AFM) images of the GO nanostructures. The thickness of the GO nanostructures was ~1 nm, as shown in Figure 1b.

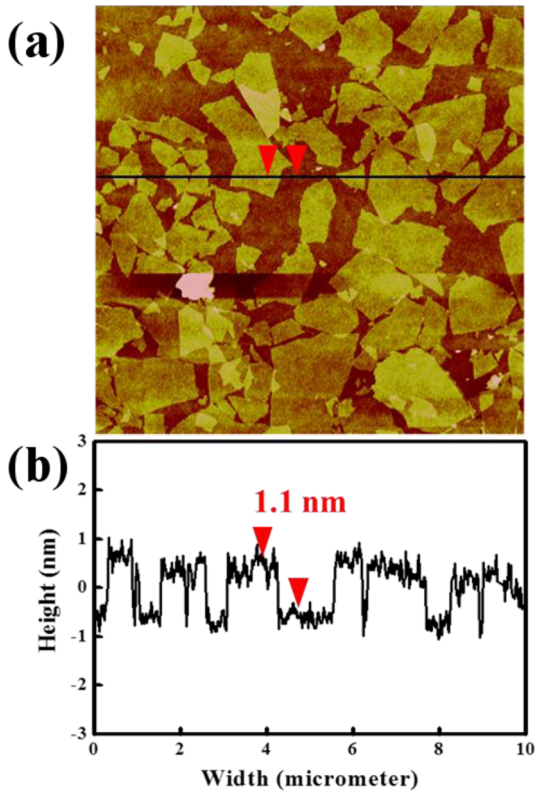

Figure 1. (a) AFM image and (b) height profile of GO nanostructures.

Further, Pt nanoparticles and GO nanostructures hybrid solution was prepared with by mixing 1 mg/mL GO nanostructures solution with 0.01 mmol/L Pt nanoparticle solution, in a ratio of 1:1 followed by ultrasonication. The size of the Pt nanoparticles is ~15 nm. This solution was first drop and dried on SiO_2/Si substrate for XPS analysis. Reduction of GO (rGO) was carried out by annealing the Pt-GO nanohybrid at 400 °C for 30 min. The chemical analysis of the Pt-GO and Pt-rGO nanohybrid were examined using X-ray photoelectron spectroscopy (XPS) (ESCA 2000, VG Microtech, U.K.) using twin anode X-ray sources Kα(1,486.6 eV)/Mg Kα (1253.6 eV) in a vacuum of 10^{-9} Torr. Figure 2a and b plots the XPS data for GO and rGO samples. The well-defined peaks for both Pt nanoparticles and GO nanostructures are marked in Figure 2a. The high resolution of Pt 4f region contains two pairs of doublets with the higher intensity doublet

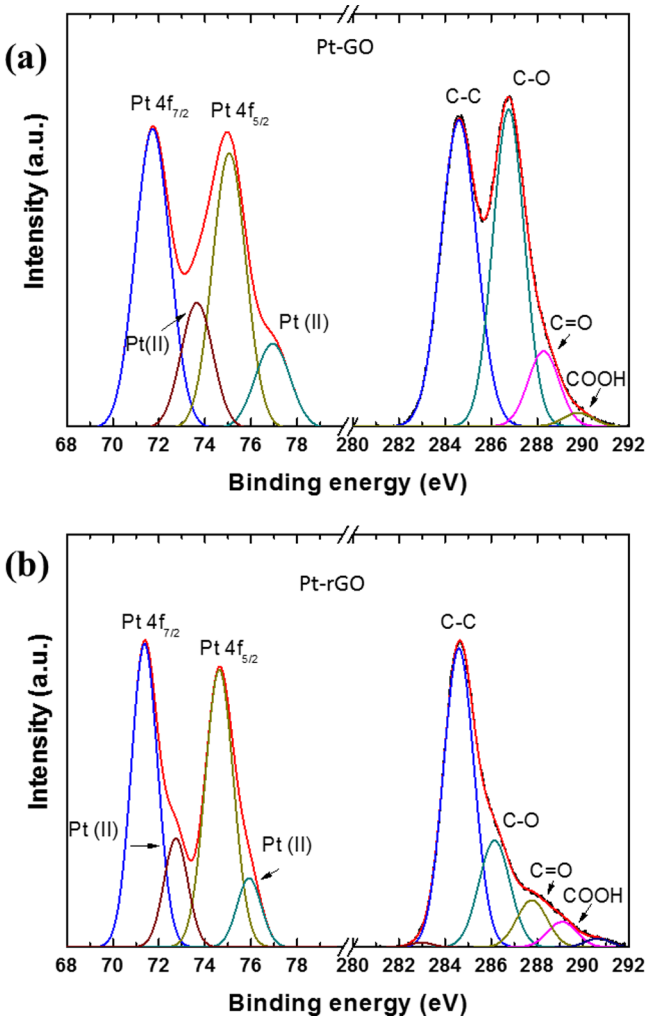

Figure 2. XPS data of Pt nanoparticles and C 1s fitted peaks of (a) GO and (b) rGO nanostructures with the peaks marked by their respective groups. Reduction in the hydroxyl, epoxy, and carboxyl peaks in rGO clearly shows the reduction of GO nanostructures.

($Pt\ 4f_{7/2}$ and $Pt\ 4f_{5/2}$) is a characteristic of metallic Pt(0) with the binding energy of 71.3 and 74.5 eV while the other doublet correspond to the Pt(II) oxidation state of Pt with the binding energy of 72.7 and 76.0 eV.[21−23] The deconvoluted C 1s peaks for GO indicates hybridized carbon, hydroxyl (C−OH, C−O), epoxy (>C═O) and carboxyl (COOH) functional groups attached to the main carbon ring at the binding energy of 284.6, 286.1, 287.5, 289.1, and 290.6, respectively.[18,19] As seen in Figure 2b, after thermal reduction, the peaks related to these functional groups decreases which confirm the reduction and partial recovery of the original graphene structure. But even after reduction, some physical damage and defects remain attached along with residual functional groups which acts as adsorption sites for gas sensing behavior.

The gas sensor device was fabricated using the DEP technique to assemble the Pt-GO nanostructures into 4 μm gap Ti/Au electrodes. Figure 3a and b show the optical microscopy images of the prepatterned Ti/Au electrodes on the Si/SiO_2 substrate. Figure 3c shows the schematic of the experimental setup for the DEP processing, with the use of a functional generator and oscilloscope. The function generator and the oscilloscope were connected to the chip by a series connection. Subsequently, 0.1 μL of mixed solution was dropped on to the electrode area. A controlled sine wave AC voltage signal was applied to the electrodes by the function generator. During the DEP process, a gradient in the electrical field was established toward the micro gap electrodes as shown by arrows in Figure 3c. This

DOI: 10.1021/acsami.5b01329
ACS Appl. Mater. Interfaces 2015, 7, 13768−13775

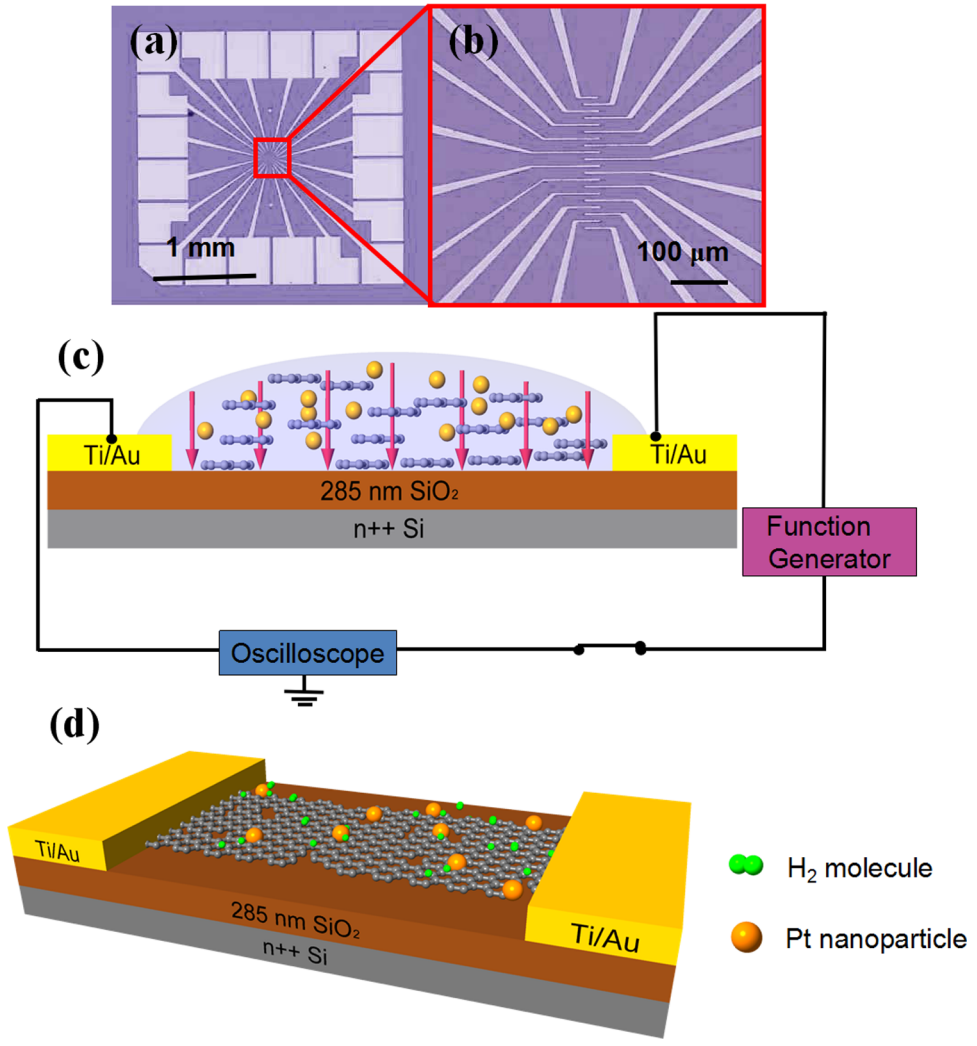

Figure 3. (a) Optical microscopy image and (b) higher magnification optical microscopy image of the prepatterned micro gap electrodes. (c) Schematic of the experimental setup for DEP processing. (d) Schematic showing assembled GO nanostructures and Pt nanoparticles between micro gap electrodes. The catalyst action of Pt nanoparticles also result in enhanced sensing response.

nonuniformity of the electric field results in the DEP force acting on nanostructure and nanoparticles floating in a medium of dielectric permittivity ε_m and can be quantitatively given by

$$\vec{F}_{DEP} = 2\pi a^3 \varepsilon_m Re[K(\omega)]\nabla E^2{}_{rms} \quad (1)$$

where a is dimension of the nanostrucuture or nanoparticle, $K(\omega)$ is the Clausius−Mossotti factor, and E_{rms} is the rms value of the electric field. Further details on this are discussed in our previous publications.[18,19]

As both GO nanostructures and Pt nanoparticles got polarized in the applied AC electric field and subsequently moves along the DEP force direction which results in the focused assembly of Pt-GO nanohybrid between the micro gap electrodes. Figure 3d illustrates GO nanostructures and Pt nanoparticles aligned between the micro gap electrodes. The aligned GO nanostructures forms an electrical connection across the electrodes when the sensing behavior can be measured and analyzed.

RESULTS AND DISCUSSION

To achieve the best result for the assembly of the Pt-decorated GO nanostructures, the optimization of the DEP parameters is most important. The controllable effective parameters include the peak-to-peak voltage (V_{pp}), frequency of applied signal, and DEP processing time. In this study, we aimed to achieve the best hydrogen gas sensing response by optimizing the DEP parameters. We tested the sensing response by varying the parameters in the following approach: various V_{pp} with a fixed frequency and processing time, various frequencies with a fixed V_{pp} and processing time, and various processing times with a fixed V_{pp} and frequency. In addition to resistance measurement, the hydrogen gas sensing behavior under several different gas concentration were tested for all DEP parameters. It may be noted that considering the complexity of optimization process, we have carried out large number of variation in the DEP parameters but only those parameters at which we have obtained a considerable change either in the sample SEM image or in the gas sensing behavior have been discussed. For sensing, the electrical measurement were carried out using Keithley 4200 SCS characterization system in a vacuum chamber in which gas flow was controlled by a gas MFC, GMC 1200 of AtoVac made. The sample was first diced and wire-bonded on a chip carrier and then mounted onto the socket in the vacuum chamber. Finally, the optimized parameters were identified based on the best sensing performance.

Figure 4a−c shows the scanning electron microscopy (SEM) (JEOL, Model JSM-7401F) images of the DEP assembled GO nanostructures, with an applied signal frequency of 500 kHz, a

DOI: 10.1021/acsami.5b01329
ACS Appl. Mater. Interfaces 2015, 7, 13768−13775

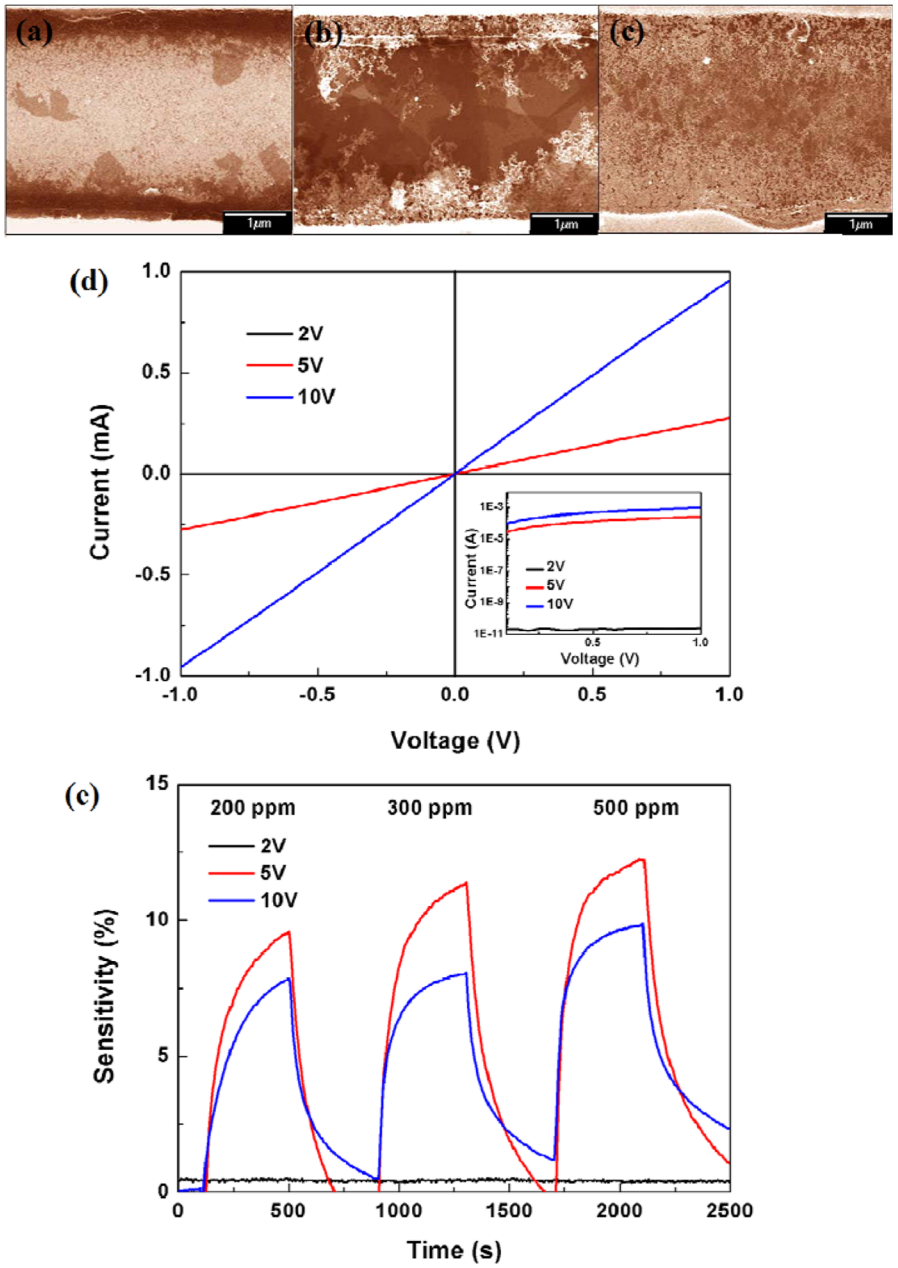

Figure 4. SEM images of the DEP-assembled Pt-decorated GO nanostructures, with 500 kHz frequency, 30 s processing time, and V_{pp} values of (a) 2, (b), 5, and (c) 10 V. The region between the electrodes is shown in panels a–c, which can be identified by the shiny metal edge visible prominently in panel c. The dark patches in panels a and b are GO flakes and the shiny aggregates are Pt nanoparticles. (d) I–V characterization and (e) hydrogen gas sensing characterization of the devices fabricated with 500 kHz frequency, 30 s processing time, and various V_{pp} values.

processing time of 30 s, and V_{pp} values of 2, 5, and 10 V, respectively. As shown in the images, the device processed under 2 V is almost disconnected between the electrodes, indicating very poor electrical conductivity. In the 5 V case, the GO nanostructures are well located between two electrodes on the sample surface and they are assembled as several bridges. In the 10 V case, the GO nanostructures and Pt nanoparticles combine with each other layer by layer. The assembled nanostructures appear as an extremely thick layer. Figure 4d shows the I–V characterization of the devices. The device fabricated with a V_{pp} of 2 V exhibits extremely poor electrical conductivity, which is consistent with the SEM image of the device in Figure 4a, whereas for 5 and 10 V the devices exhibit well connection as seen from the electrical response in Figure 4d. Figure 4e demonstrates the hydrogen gas sensing characterization of the devices fabricated with a frequency of 500 kHz, processing time of 30 s, and various V_{pp} values, at hydrogen gas concentrations of 200, 300, and 500 ppm. To determine the quality of the sensing response of the gas sensor device, the most important attribute is sensitivity. The sensitivity (S) is defined by the equation

$$S = (R - R_0)/R_0 \times 100\% \quad (2)$$

where R is the device resistance in the target gas environment and R_0 is the device resistance in the environment without the target gas. Of all the devices, the device fabricated with a frequency of 500 kHz, a processing time of 30 s, and a V_{pp} of 5 V demonstrates the best sensitivity to hydrogen gas for all three

DOI: 10.1021/acsami.5b01329
ACS Appl. Mater. Interfaces 2015, 7, 13768–13775

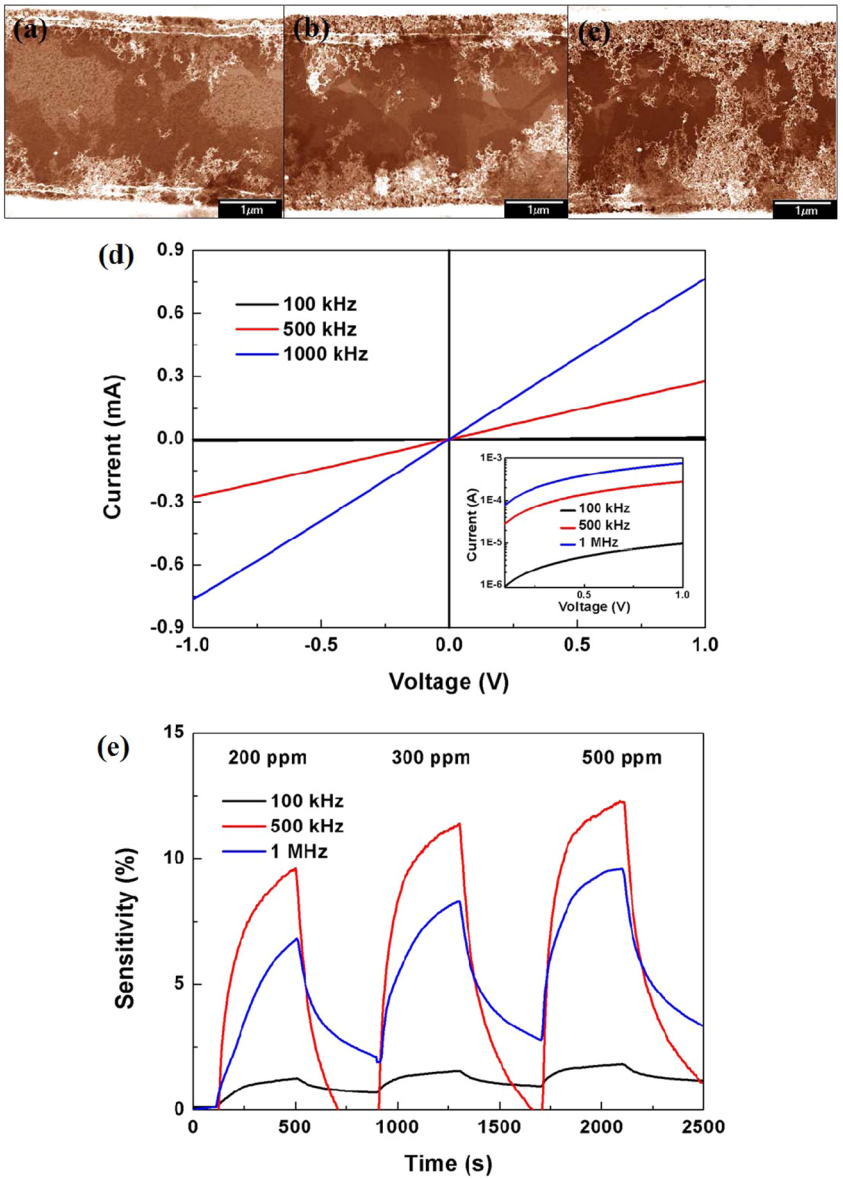

Figure 5. SEM images of the DEP assembled Pt-decorated GO nanostructures with a V_{pp} of 5 V, 30 s processing time, and (a) 100 kHz, (b), 500 kHz, and (c) 1 MHz applied frequencies. (d) *I*−*V* characterization and (e) hydrogen gas sensing characterization of the devices fabricated with a V_{pp} of 5 V, 30 s processing time, and various applied frequencies.

devices. The device could achieve 10% sensitivity for 200 ppm hydrogen gas at room temperature. Before discussing further DEP optimization, a brief view of sensing mechanism is described here: rGO nanostructures have defect sites and broken graphene rings, which adsorb hydrogen molecules and subsequently affect the electrochemical potential of the structure, which results in the variation of its electrical properties. The magnitude of this variation depends on various factors including the intensity of the defect sites, remaining chemically active -hydroxyl and -carboxyl groups in the nanostructures, etc. With the addition of Pt nanoparticles, this sensing mechanism is enhanced further because of the catalytic action of Pt nanoparticles which dissociate molecular hydrogen on their surface and adsorb the hydrogen atoms to form hydrides, PtH_x. Further, the spill of excess dissociate hydrogen molecules got adsorbed on the adjacent rGO nanostructures which results in an enhanced sensing behavior. This enhancement due to the Pt nanoparticles can be compared directly with the previous published result[19] where only rGO device fabricated with similar DEP parameter (5 V, 50 kHz, and 30 s) shows just 5% sensing behavior at room temperature for 200 ppm hydrogen. Whereas with Pt nanoparticles, the nanohybrid of Pt-rGO shows a 100% enhancement with 10% sensitivity. This shows that the DEP assembly of Pt-rGO nanohybrid is an efficient way to improve the sensing performance. Further, it would be interesting to note here that a similar device fabricated only with rGO without DEP process showed a comparatively lesser sensitivity than a similar DEP assembled device (5 V, 50 kHz, and 30 s).[10]

Figure 5a−c shows the SEM images of the GO nanostructures assembled using the DEP technique with a V_{pp} of 5 V, processing time of 30 s, and applied frequencies of 100, 500, and 1000 kHz, respectively. It can be observed that the devices are satisfactorily assembled with good connections for higher frequencies. However, as the frequency increased, the thickness of the GO nanostructure layer and the density of the

DOI: 10.1021/acsami.5b01329
ACS Appl. Mater. Interfaces 2015, 7, 13768−13775

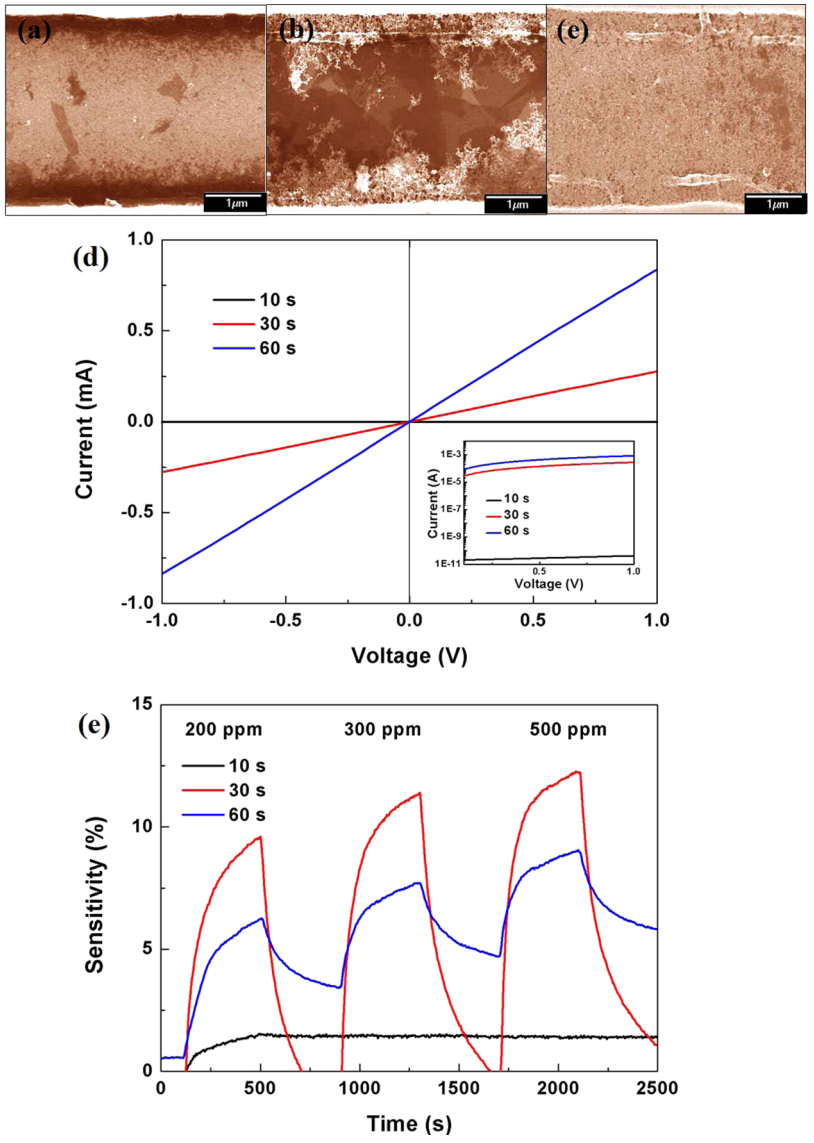

Figure 6. SEM images of the DEP assembled Pt-decorated GO nanostructures with a V_{pp} of 5 V, 500 kHz applied frequency, and processing times of (a) 10, (b), 30, and (c) 60 s. (d) $I-V$ characterization and (e) the hydrogen gas sensing characterization of the devices fabricated with a V_{pp} of 5 V, 500 kHz applied frequency, and various processing times.

Pt nanoparticles also increased. Figure 5d shows the $I-V$ characterization of the devices where a correlation between the better assembled nanostructures and improved electrical behavior can be seen clearly. Figure 5e demonstrates the hydrogen gas sensing characterization of the devices fabricated with a V_{pp} of 5 V, a processing time of 30 s, and various applied frequencies, at hydrogen gas concentrations of 200, 300, and 500 ppm, respectively. The device fabricated with an applied frequency of 500 kHz, a processing time of 30 s, and a V_{pp} of 5 V exhibits the best sensitivity to hydrogen gas for all three devices. It may be interested to note here that contrary to the apparent assumption, the least resistive device does not show the best sensitivity as can be seen in the previous result for V_{pp} optimization. The reason behind this is that the least resistive device, as can be seen in Figure 4c and 5c, consist of multiple rGO layers number and an increase density of Pt nanoparticles. With thicker rGO layers the 2D behavior of rGO is compromised because the sensing response of the underlying layers got screened by the upper layers, thereby the modulation in electrical behavior due to hydrogen adsorption shows lesser response hence lower sensitivity.

Figure 6a–c shows the SEM images of the GO nanostructures assembled using the DEP technique with a V_{pp} of 5 V, an applied frequency of 500 kHz, and processing times of 10, 30, and 60 s, respectively. The device fabricated with a processing time of 10 s had no connection, as shown in the images. The device fabricated with a processing time of 30 s was almost entirely covered and connected well by GO nanostructures and Pt nanoparticles between the electrodes. However, for 60 s, the assembled layer appears to be thick film and acquire vertical dimension. Figure 6d shows the $I-V$ characterization of the devices where it can be seen that current increases with increase in assembly time reaching maximum value for 60 s. Figure 6e demonstrates the hydrogen gas sensing characterization of the devices fabricated with a V_{pp} of 5 V, an applied frequency of 500 kHz, and various processing times, at hydrogen gas concentrations of 200, 300, and 500 ppm. As demonstrated in the figure, the device fabricated with a

DOI: 10.1021/acsami.5b01329
ACS Appl. Mater. Interfaces 2015, 7, 13768–13775

frequency of 500 kHz, processing time of 30 s, and V_{pp} of 5 V exhibits the best sensitivity to hydrogen gas for all three devices.

As shown in Figures 4−6, the device fabricated with a V_{pp} of 5 V, an applied frequency of 500 kHz, and a processing time of 30 s exhibits highest sensing response to hydrogen gas. In the case of different conditions like lower V_{pp} value (2 V), lower applied frequency (100 kHz), and shorter processing time (10 s), there is barely any connection or a very poor connection, resulting in very poor electrical conductivity and very poor gas sensitivity of the device. However, with higher V_{pp} value (10 V) or higher applied frequency (1000 kHz), or longer processing time (60 s), the assembled GO nanostructures were thicker and the Pt nanoparticles were denser than the device fabricated with the intermediate values. As discussed previously that the thicker layer and the higher particle density lower the surface-to-volume ratio of the nanostructures which results in lower sensitivity. Previous reports also demonstrated that a higher surface-to-volume ratio lead to increase gas sensing response.[18,19] Besides particle density and thickness of GO layers, nanoparticles size can also affect the sensing performance; however, because of material constraints, such study could not be carried out in the present study.

Figure 7 summarize the sensitivity and resistance variation for all devices with various DEP parameters. As seen from the

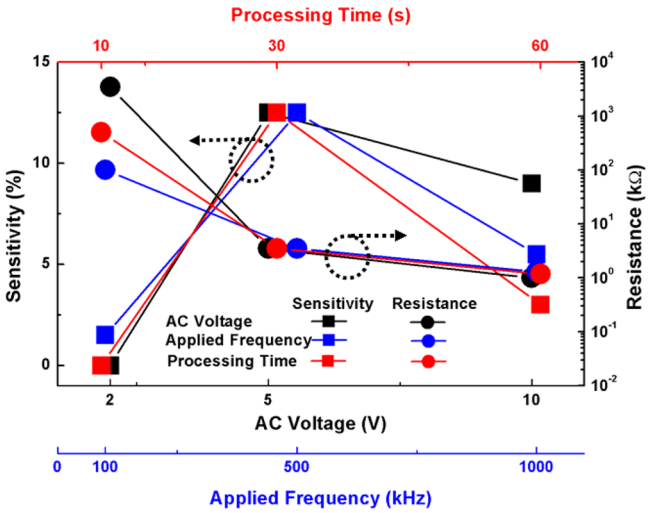

Figure 7. Variation in sensitivity and resistance of the sensor device for different DEP parameters for 500 ppm hydrogen gas concentration.

figure, the device with optimized DEP parameters of 5 V, 500 kHz, and 30 s gives the best sensitivity. It can be seen that the resistance of the fabricated devices decreases with the individual increase in all DEP parameters like V_{pp}. A.C. frequency and deposition or DEP time. However, the sensitivity response peaks only at the optimized parameter and drops for both most and least resistive devices due to the inconsistence connection for the former and thicker rGO deposition for the latter case. Therefore, it is an important observation that the resistance of the rGO-Pt nanohybrid sensors is not the sole criteria to predict the sensor performance.

To analysis the in depth sensing behavior, Figure 8 plot the response and recovery time for different DEP parameters conditions at various gas concentrations, where the time required for the response to reach up to 90% of its peak value defines response time and the time required for the response to decrease from 90% of its highest value to its initial value is

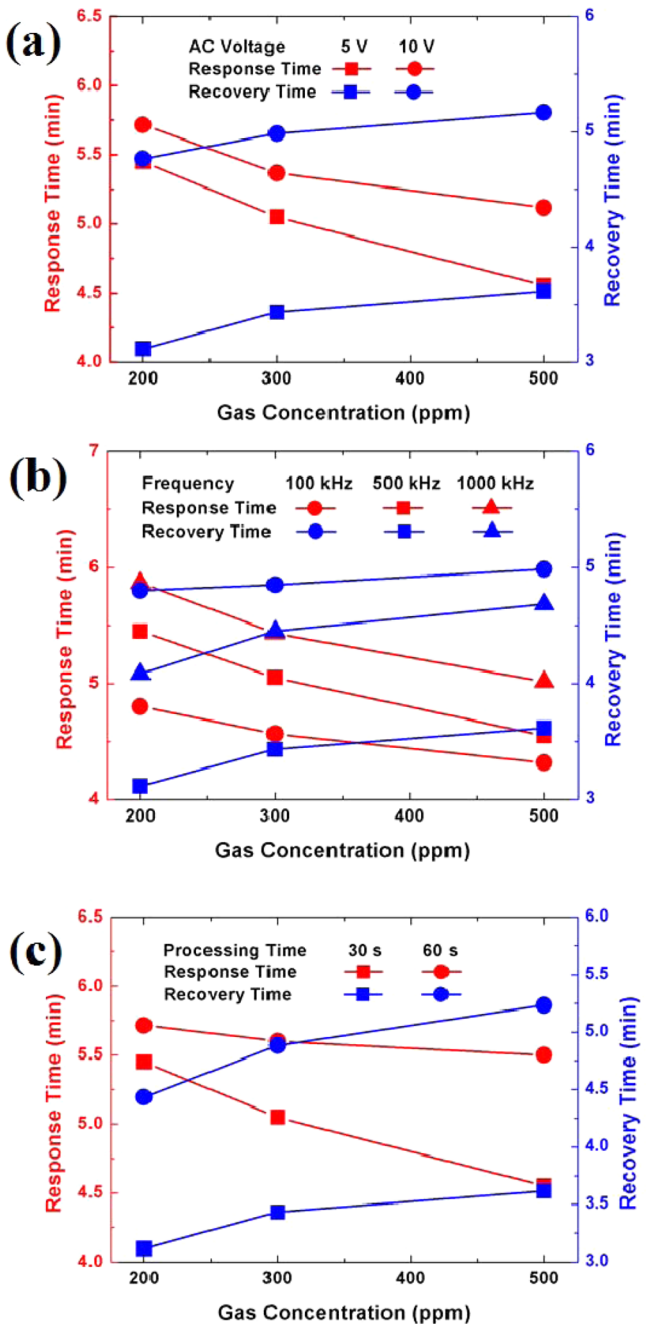

Figure 8. Response time and recovery time of the sensor device fabricated based on (a) various V_{pp}, (b) various applied frequency, and (c) various processing time, respectively.

termed as recovery time. As seen in Figure 8a that both response and recovery time decrease with an increase in V_{pp} from 5 to 10 V, this decrease can be related to better assembly and sensitivity of the sample at 5 V. However, with increase in gas concentration, response and recovery time exhibit opposite behavior, where the former improves while the latter degrades. The improvement in response time can be explained from the fact that the high concentration of the gas leads to a higher change in resistance, thus comparatively smaller time whereas the recovery time increases because of increase in adsorption of the gas molecules on the defect sites on rGO and Pt NPs as well, which results in the increase in deadsorption time. Similar explanation holds valid for the response and recovery time

DOI: 10.1021/acsami.5b01329
ACS Appl. Mater. Interfaces 2015, 7, 13768−13775

behavior observed in Figure 8b and 8c, for DEP frequency and deposition time, respectively. However, the sample with 100 kHz in Figure 8b shows a marginally better response time as compared to other conditions but the optimized sensor shows the least recovery time. Although, the response and recovery time observed in this work are higher than the industrial standards but they showed improvement over the other published results.[10,11] Finally, the reliability and reproducibility of the sensors studied in this study were found to be satisfactory and the sensing performance was also found to be stable enough with negligible variations even after several weeks.

CONCLUSION

In this study, we optimized the DEP assembly technique to fabricated highly sensitive hydrogen gas sensor based on Pt-decorated GO nanostructures. The DEP parameters of V_{pp}, applied frequency, and processing time were optimized. The device with the best sensing response to hydrogen gas was fabricated with parameters of 5 V, 500 kHz, and 30 s, respectively. By applying the optimized parameters, the assembled device could achieve ~10% sensitivity to 200 ppm hydrogen gas at room temperature.

AUTHOR INFORMATION

Corresponding Author

*E-mail: ghkim@skku.edu.

Author Contributions

⊥J.W. and S.R. contributed equally to the work.

Notes

The authors declare no competing financial interest.

ACKNOWLEDGMENTS

This research was supported by Basic Science Research Program through the National Research Foundation of Korea (NRF) funded by the Ministry of Education, Science and Technology (2013R1A2A2A01069023).

REFERENCES

(1) Crabtree, G. W.; Dresselhaus, M. S.; Buchanan, M. V. The Hydrogen Economy. *Phys. Today* **2014**, *57*, 39.

(2) Zhang, H.; Feng, J. C.; Fei, T.; Liu, S.; Zhang, T. SnO_2 Nanoparticles Reduced Graphene Oxide Nanocomposites for NO_2 Sensing at Low Operating Temperature. *Sens. Actuators B* **2014**, *190*, 472−478.

(3) Baik, J. M.; Kim, M. H.; Larson, C.; Yavuz, C. T.; Stucky, G. D.; Wodtke, A. M.; Moskovitis, M. Pd-Sensitized Single Vanadium Oxide Nanowires: Highly Responsive Hydrogen Sensing Based on the Metal-Insulator Transition. *Nano Lett.* **2009**, *9*, 3980−3984.

(4) Kwak, Y.; Wang, J.; Meang, S.; Kim, G.-H. Hydrogen Sensing Properties of Dielectrophoretically Assembled SnO_2 Nanoparticles on CMOS-Compatible Micro-hotplates. *Nanotechnology* **2011**, *22*, No. 445501.

(5) Dag, S.; Ozturk, Y.; Ciraci, S.; Yildirim, T. Adsorption and Dissociation of Hydrogen Molecules on Bare and Functionalized Carbon Nanotubes. *Phys. Rev. B* **2005**, *72*, No. 155404.

(6) Sayago, I.; Terrado, E.; Lafuente, E.; Horrillo, M. C.; Maser, W. K.; Benito, A. M.; Navarro, R.; Urriolabeitia, E. P.; Martinez, M. T.; Gutierrez, J. Hydrogen Sensors Based on Carbon Nanotubes Thin Films. *Synth. Met.* **2005**, *148*, 15−19.

(7) Kong, J.; Chapline, M. G.; Dai, H. Functionalized Carbon Nanotubes for Molecular Hydrogen Sensors. *Adv. Mater.* **2001**, *13*, 1384−1386.

(8) Schedin, F.; Geim, A. K.; Morozov, S. V.; Hill, E. W.; Blake, P.; Katsnelson, M. I.; Novoselov, K. S. Detection of Individual Gas Molecules Adsorbed on Graphene. *Nat. Mater.* **2007**, *6*, 652−655.

(9) Gautam, M.; Jayatissa, A. H. Graphene Based Field Effect Transistor for the Detection of Ammonia. *Appl. Phys. Lett.* **2012**, *112*, 064304.

(10) Wang, J.; Kwak, Y.; Lee, I. Y.; Maeng, S.; Kim, G.-H. Highly Responsive Hydrogen Gas Sensing by Partially Reduced Graphite Oxide Thin Films at Room Temperature. *Carbon* **2012**, *50*, 4061−4067.

(11) Lu, G.; Park, S.; Yu, K.; Ruoff, R. S.; Ocola, L. E.; Rosenmann, D. Towards Practical Gas Sensing with Highly Reduced Graphene Oxide: A New Signal Processing Method to Circumvent Run-to-Run and Device-to-Device Variations. *ACS Nano* **2011**, *5*, 1154−1164.

(12) Kumar, S.; Seo, Y. K.; Kim, G.-H. Manipulation and Trapping of Semiconducting ZnO Nanoparticles into Nanogap Electrodes by Dielectrophoresis Technique. *Appl. Phys. Lett.* **2009**, *94*, No. 153104.

(13) Cheon, D.; Kumar, S.; Kim, G.-H. Assembly of Gold Nanoparticles of Different Diameters between Nanogap Electrodes. *Appl. Phys. Lett.* **2010**, *96*, No. 013101.

(14) Krupke, R.; Linden, S.; Rapp, M.; Hennrich, F. Thin Films of Metallic Carbon Nanotubes Prepared by Dielectrophoresis. *Adv. Mater.* **2006**, *18*, 1468−1470.

(15) Asokan, S. B.; Jawerth, J.; Carroll, R. L.; Cheney, R. E.; Washburn, S.; Sperfine, R. Two-Dimensional Manipulation and Orientation of act In-myosin Systems with Dielectrophoresis. *Nano Lett.* **2003**, *3*, 431−437.

(16) Guo, Y.; Wu, B.; Liu, H.; Ma, Y.; Yang, Y.; Zheng, J.; Yu, G.; Liu, Y. Electrical Assembly and Reduction of Graphene Oxide in a Single Solution Step for Use in Flexible Sensors. *Adv. Mater.* **2011**, *23*, 4626−4630.

(17) Tuukkanen, S.; Toppari, J. J.; Kyzyk, A.; Hirviniemi, L.; Hytonen, V. P.; Ihalainen, T.; Torma, P. Carbon Nanotubes as Electrodes for Dielectrophoresis of DNA. *Nano Lett.* **2006**, *6*, 1339−1343.

(18) Wang, J.; Singh, B.; Maeng, S.; Joh, H.-I.; Kim, G.-H. Assembly of Thermally Reduced Graphene Oxide Nanostructures by Alternating Current Dielectrophoresis as Hydrogen-Gas Sensors. *Appl. Phys. Lett.* **2013**, *103*, No. 083112.

(19) Wang, J.; Singh, B.; Park, J.; Rathi, S.; Lee, I.-Y.; Maeng, S.; Joh, H.-I.; Lee, C.-H.; Kim, G.-H. Dielectrophoresis of Graphene Oxide Nanostructures for Hydrogen Gas Sensor at Room Temperature. *Sens. Actuators B* **2014**, *194*, 296−302.

(20) Hirata, M.; Gotou, T.; Horiuchi, S.; Fujiwara, M.; Ohba, M. Thin-Film Particles of Graphite Oxide 1: High-yield Synthesis and Flexibility of the Particles. *Carbon* **2004**, *42*, 2929−2937.

(21) Xu, J.; Liu, X.; Chen, Y.; Zhou, Y.; Lu, T.; Tang, Y. Platinum−Cobalt Alloy Networks for Methanol Oxidation Electrocatalysis. *J. Mater. Chem.* **2012**, *22*, No. 23659.

(22) Sen, F.; Karatas, Y.; Gulcan, M.; Zahmakiran, M. Amylamine Stabilized Platinum(0) Nanoparticles: Active and Reusable Nanocatalyst in the Room Temperature Dehydrogenation of Dimethylamine-Borane. *RSC Adv.* **2014**, *4*, 1526.

(23) Yue, B.; Ma, Y.; Tao, H.; Yu, L.; Jian, G.; Wang, X.; Wang, X.; Lu, Y.; Hu, Z. CNx Nanotubes as Catalyst Support to Immobilize Platinum Nanoparticles for Methanol Oxidation. *J. Mater. Chem.* **2008**, *18*, 1747−1750.

DOI: 10.1021/acsami.5b01329
ACS Appl. Mater. Interfaces 2015, 7, 13768−13775